Proof of Concept of Impedance Control on a Didactic Manipulator

Felipe Augusto Rizzi * **Gabriel Alencar Jeronimo Antonio** **
Bruno Augusto Angelico ***

Escola Politécnica, Universidade de São Paulo, SP

* *e-mail: felipe.rizzi@usp.br*
** *e-mail: gabriel.antonio@usp.br*
*** *e-mail: angelico@usp.br*

Abstract: Traditionally, the control of manipulators targets position or force tracking and numerous well succeed and high precision solutions have been developed over the last decades. However, for some applications, single force or position control are not efficient, and a specified relationship between both must be imposed. This paper describes the implementation of impedance control technique over a didactic manipulator, as a proof of concept.The performance achieved is limited by the quality and number of axis of force measurement, as well as the quality of actuators.

Keywords: Position Control; Impedance control; Interaction Control; Robotic Manipulation; Simulation.

1. INTRODUCTION

Robotic manipulators have been widely used in industry since the late 1970s, allowing the automation of various tasks previously performed by humans, such as painting, welding and transportation.

In conventional applications, it is desired that some vector quantity associated with the manipulator's extremity, such as velocity, position or force, tracks a reference (Craig, 2013). However, it is impossible to control both variables associated with displacements (e.g. position, velocity) and variables associated with efforts (e.g. force, torque) simultaneously, in the same direction, as a consequence of the interdependence between them, imposed by the laws of dynamics for rigid bodies.

Another key feature in classical applications, as shown in (Corke, 2017), is the modelling of interactions with the external environment as disturbances . Thus, the control action seeks to neutralize the effect caused by the contact forces exchanged between the environment and the manipulator, in order to achieve the control objective. However, conventional control techniques are not effective for certain applications, where the interaction between manipulator and environment is part of the control objective itself.

A first example where interaction control is relevant is in the field of mobile robotics. Locomotion in rough terrain is a major challenge for robots with legs, as the contact point between a leg and the ground is inaccurate and tends to suffer deformations during interaction. In this context, it is desirable that the robot's legs have a certain elastic behavior, preventing it from becoming unbalanced. In (Faigl and Čížek, 2019), impedance control has been applied to a hexapod robot.

Interaction control is also essential in the field of cobotics, where humans and robots must work together to carry out a task. This subject has been extensive studied in (Ikeura and Inooka, 1995). The cooperation has many obstacles within the classical control paradigm, as a collision between a robot and a human is interpreted as a disturbance to be rejected, which makes the work environment extremely unsafe.

The last example is in robotic-assisted surgery, where surgical robots, operated remotely by doctors, need to manipulate extremely soft organs and tissues, as in (Sharifi et al., 2018). The difference between operator movements responsible for simply holding an organ or crushing it is subtle, making it difficult to distinguish between them without interaction control.

The previous examples highlight the need to control the interaction between the manipulator and the environment and present some desirable qualitative characteristics for each type of interaction. The impedance control (Hogan, 1984), explored in this work, is an adequate technique for the previous cases and aims to impose a relationship between the contact force and the displacement of the manipulator (Song et al., 2019), instead of controlling only one of these variables, as in conventional control techniques.

The rest of this paper has the following organization: section 2 describes technical background behind impedance control; section 3 presents the definitions adopted in this project; section 4 resumes the development of force sensor and sections 5 and 6 present design key features and results for position and impedance control loops, respectively. Section 7 draws conclusions from the work.

2. BACKGROUND

Controlling the interaction between a manipulator and the environment is a purpose that precedes impedance control. In (Raibert and Craig, 1981), a technique called "hybrid force and position control" was presented, where the position of an end-effector restrained to a surface and the normal force to this surface were controlled simultaneously. Notice that this is physically possible, as the force-controlled and position-controlled directions are orthogonal.

The technique of impedance control was first presented in (Hogan, 1984) and lies on the concept of mechanical impedance. In physical modelling, one can classify variables in two different groups:

- **Flow variables**: These variables are related to some material flow in the system. Examples: velocity, angular velocity, current, flow.
- **Effort variables**: These variables put the system in action. The product between an effort variable and its respective flow variable gives the instant power consumed by the system. Examples: force, torque, voltage, pressure.

Concerning the causality, if the input of the system is an effort variable and its output is as a flow variable, it is said to be an "admittance". The other possibility is a system with a flow variable input and an effort variable output, which is an "impedance".

In robotics, it is suitable to model the environment as an admittance, as the impedance representation does not allow to determine uniquely the applied force. For instance, a zero displacement is associated to a null force, in the trivial case, but it is also possible that a non zero force does not induce displacement in a rigid environment (wall collision). Consequently, the manipulator must be represented as an impedance, which explains the name of the technique addressed in this work.

The goal of impedance control, in its most popular formulation, is to impose a relationship between the contact effort vector $\mathbf{F}_{ext} \in \mathbb{R}^6$, whose components are interaction forces and torques exerted by the manipulator on the environment, and the displacement vector $\Delta\mathbf{x} \in \mathbb{R}^6$, whose components are linear and angular displacements. The displacement vector $\Delta\mathbf{x}$ is the difference between the actual position and orientation of the end-effector $\mathbf{x}(t)$ and the virtual trajectory $\mathbf{x}_v(t)$, which is the trajectory performed in the absence of interaction, as represented in figure 1:

The desired relationship between $\mathbf{F}_{ext}$ and $\Delta\mathbf{x}$ is usually given by (1):

$$-\mathbf{F}_{ext}(t) = \mathbf{K}\Delta\mathbf{x}(t) + \mathbf{B}\Delta\dot{\mathbf{x}}(t) + \mathbf{M}\Delta\ddot{\mathbf{x}}(t) \quad , \qquad (1)$$

where $\mathbf{K}$, $\mathbf{B}$ and $\mathbf{M}$ are 6×6 matrices. Notice that these matrices are diagonal in the decoupled case, whose dynamics in each direction is equivalent to a one-dimensional damped mass-spring system.

Different topologies for implementing the relationship of (1) are described in the literature. The first one, called

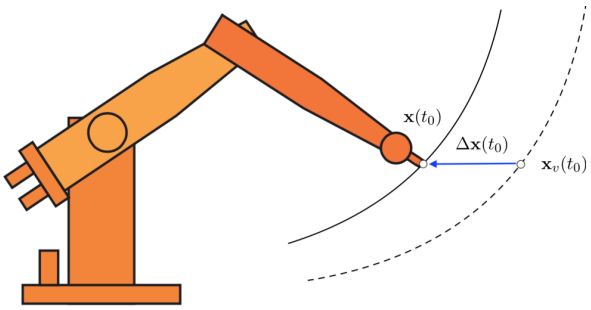

Figure 1. Representation of real and virtual trajectories. (Craig, 2013) - modified.

"position-based", assumes the existence of a conventional position control loop, over which an impedance loop is built. In (Richardson et al., 2005), the position-based implementation was used in a physiotherapist robot application.

The second topology, called "torque-based", considers an inner force/torque loop and outer impedance loop. In (Jutinico et al., 2017), this implementation was successfully applied to an ankle rehabilitation robot.

The last topology, called "model-based", considers both the impedance model and the manipulator dynamic model for control law design. A complete review of these three techniques is provided in (Song et al., 2019).

3. PROJECT DEFINITIONS

In this work, the control impedance technique was applied to the 4 degrees of freedom RRR didactic manipulator presented in figure 2. The configuration of joint angles (θ_1, θ_2, θ_3 and θ_4) can be visualized in figure 3.

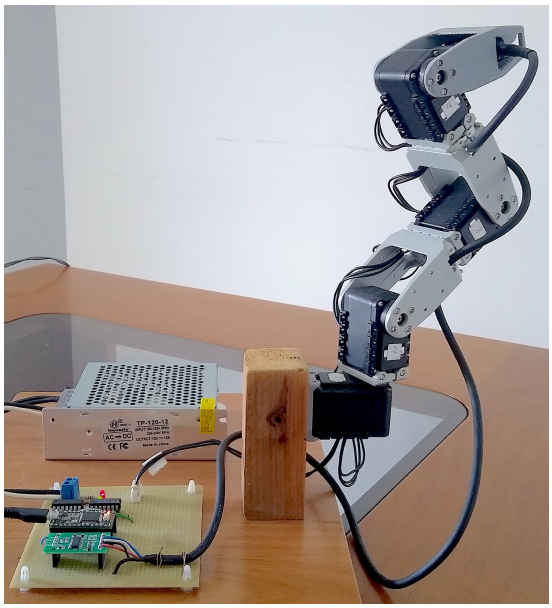

Figure 2. Didactic manipulator used in this work.

This manipulator was subjected to the material constraints imposed by the resources available at the Applied Control Laboratory (LCA), such as:

- Use of Dynamixel AX-12A servomotors as actuators;

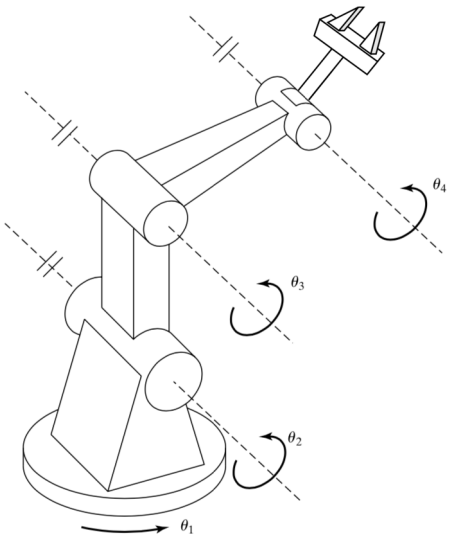

Figure 3. Joint angles configuration. (Craig, 2013) - modified.

- Use of Teensy 3.2 USB micro-controller development board to implement digital control laws;
- Use of Bioloid robot parts and 3D printed links for mechanical structure.

Since servomotors present a built-in position control, the position-based implementation, depicted in figure 4, was chosen for this project.

In figure 4, the Cartesian displacement vector $\Delta\mathbf{x}$ is computed from measured effort $\mathbf{F}_{ext}$ with (1), called "Impedance model". The Cartesian position reference $\mathbf{x}_c$ is obtained by summing $\Delta\mathbf{x}$ to the virtual trajectory reference $\mathbf{x}_v$ and then converting it to the angular vector reference $\mathbf{\Theta}_c$, in joint space. Finally, the position control loop receives $\mathbf{\Theta}_c$ and imposes the angular positions $\mathbf{\Theta}$ to the manipulator joints.

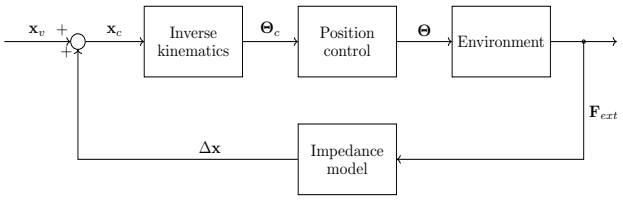

Figure 4. Position-based implementation.

4. FORCE SENSOR

The customized proof-of-concept single axis force sensor shown in figure 5 has been developed to enable the posion-based implementation of impedance control.

The sensor is based on the double-cantilever-beam structure shown in figure 6, which presents a surface strain ε proportional to the measured force F, aligned to the measurement axis. Figure 7 presents the strains obtained by finite element analysis, when a force $F = 10\,\text{N}$ is applied.

In order to convert strains into electrical signals, a full-bridge strain gauge topology has been adopted. In figure 8, red and blue rectangles represent the position of strain

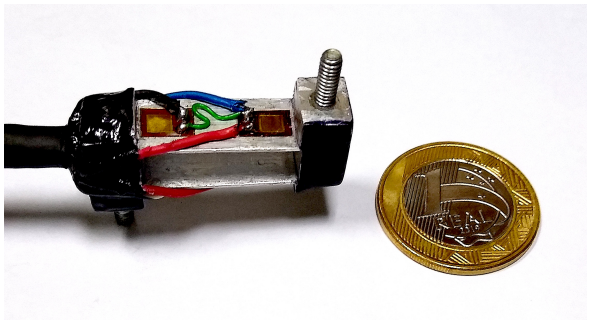

Figure 5. Force sensor.

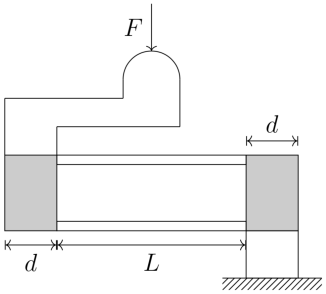

Figure 6. Sensor cross section. $F = 10\,\text{N}$. L and d are structure dimensions.

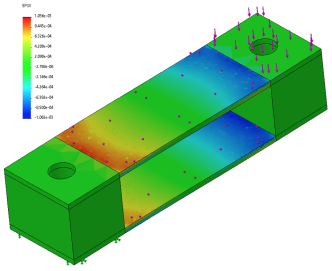

Figure 7. Finite elements strain analysis. $\varepsilon = 1.06 \times 10^{-3}\,\text{N}$.

gauges subjected to compression and extension, respectively, when a compression force f_1 is applied. Figure 8 also presents the equivalent electrical circuit, where R is the nominal strain gauge resistance and ΔR the strain-related resistance variation.

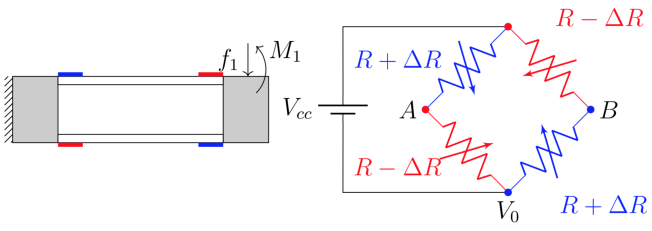

Figure 8. Strain gauges positions and equivalent electrical circuit.

The voltage V_{BA} between points B and A, proportional to the strain ε, has been sampled with a HX711 ADC module and the sensor has been calibrated subsequently.

In figure 9, applied and measured forces in a static test are shown. The basic performance specifications extracted

from figure 9 are ±10 N range and ±0.03 N measurement precision.

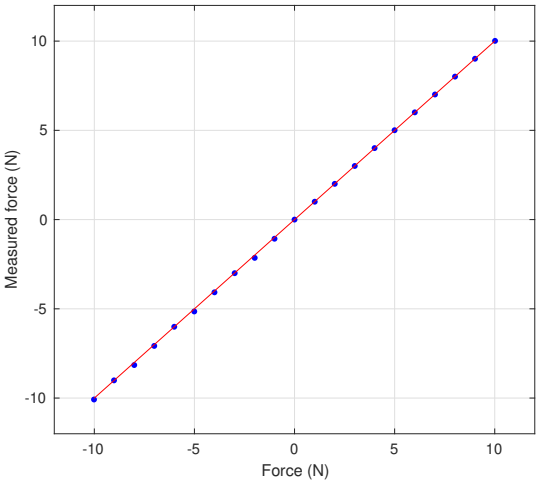

Figure 9. Sensor static test. The red line is the identity function, and blue markers are measurements corresponding to decreasing loads.

5. POSITION LOOP

5.1 Design

The position loop design started with the development of kinematic and dynamic models to describe the manipulator behaviour. The dynamic model, obtained from Lagrangian mechanics equations, is shown in (2):

$$\tau_{act} - \tau_{ext} = \mathbf{H}(\mathbf{\Theta})\ddot{\mathbf{\Theta}} + \mathbf{V}(\mathbf{\Theta}, \dot{\mathbf{\Theta}}) + \mathbf{G}(\mathbf{\Theta}) + \mathbf{F}(\mathbf{\Theta}, \dot{\mathbf{\Theta}}) \quad , \quad (2)$$

where $\mathbf{H}(\mathbf{\Theta})$ is the inertia matrix and $\mathbf{V}(\mathbf{\Theta}, \dot{\mathbf{\Theta}})$, $\mathbf{G}(\mathbf{\Theta})$, $\mathbf{F}(\mathbf{\Theta}, \dot{\mathbf{\Theta}})$, τ_{act} and τ_{ext} are the Coriolis/centrifugal, gravitational, friction, actuator and external joint torques, respectively.

Most part of the model parameters has been derived from CAD model, except the friction coefficients, determined by identification. A Matlab/Simulink model has been implemented subsequently, in order to perform numeric simulations.

Concerning the position control topology, an independent joint control has been adopted, since servomotors present a proportional built-in position controller (ROBOTIS, 2021), described by (3):

$$u(t) = K(r(t) - \theta(t)) \quad , \quad (3)$$

where $r(t), K, u(t)$ and $\theta(t)$ are, respectively, the setpoint, proportional gain, motor torque and measured angle. All variables refer to one of the four joints.

The performance of position loop has been enhanced by the addition of an external integrator to the built-in controller input (Shao et al., 2015), in order to eliminate the steady state error for constant setpoints, caused by gravitational torques and Coulomb friction. Equation (4) gives the expression to $r(t)$ considering the external integral action:

$$r(t) = \theta_c(t) + K_I{}' \int_0^t (\theta_c(\tau) - \theta(\tau))d\tau \quad , \quad (4)$$

where $\theta_c(t)$ and $K_I{}'$ are, respectively, the new setpoint and the integrator gain.

Combining (3) and (4), it becomes clear that the overall controller has a proportional integral law, as shown in (5):

$$u(t) = K(\theta_c(t) - \theta(t)) + K_I \int_0^t (\theta_c(\tau) - \theta(\tau))d\tau \quad , \quad (5)$$

where $K_I = KK_I{}'$.

It is important to remark that integrators with anti-windup clamp systems have been deployed, in order to deal with torque saturation within actuators. The continuous control law has been discretized and implemented digitally with a sampling frequency of 40 Hz.

The position controller tuning methodology consisted in selecting the servomotor's proportional gain K responsible for the fastest time response without excessive flutter, preventing mechanical structure damage. Then, $K_I{}'$ value was regulated to minimize the position error vanishing time, without an aggressive response. The global stability can be proved thanks to saturations (Yarza et al., 2011), and is also verified through simulation.

The optimal value obtained via simulation was $K_I^{'} = 1.5\,\mathrm{s}^{-1}$ and the one that generated the best performance was $K_I^{'} = 1.0\,\mathrm{s}^{-1}$, verifying the model representativeness.

5.2 Results

Figures 10 and 11 contain, respectively, the four joint angle responses and tracking errors for a given test trajectory. In Figure 10, the crosses, representing the measures, are close to the dashed and solid lines, representing setpoints and simulation outputs, indicating a good trajectory tracking as well as a good model-reality match. In Figure 11, the maximum recorded tracking error is 2°, what corresponds to a good performance, considering the precision of 0.29° for angle measurements.

6. IMPEDANCE LOOP

6.1 Design

Since the manipulator has four degrees of freedom, the effort and displacement vectors in (1) belong to a 4-dimensional space and can be uniquely described in terms of four-coordinate tuples. The three first chosen coordinates in the position vector correspond to the Cartesian coordinates x, y, z and the fourth one is the orientation angle ϕ of manipulator's end effector, such that $\phi = \theta_2 + \theta_3 + \theta_4$. The components of effort vector correspond to the respective Cartesian forces F_x, F_y and F_z and τ_ϕ, which is the torque applied on the rotational axis of ϕ.

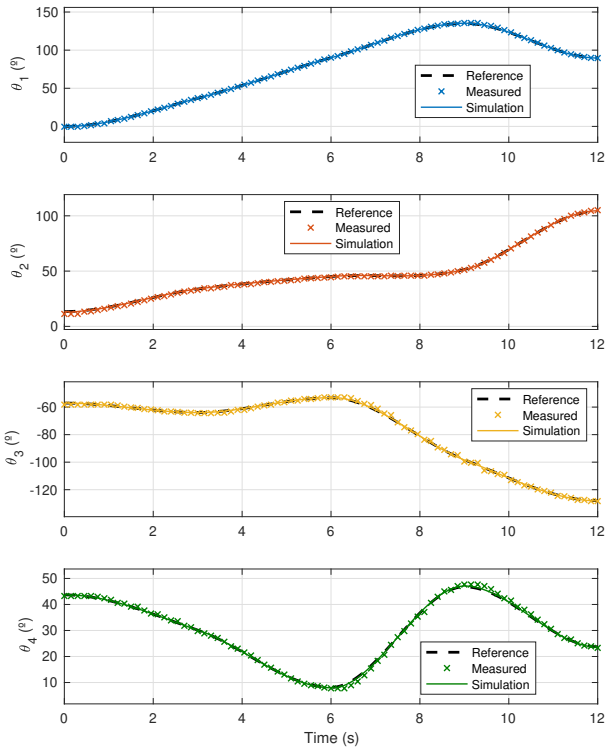

Figure 10. Joint angle responses.

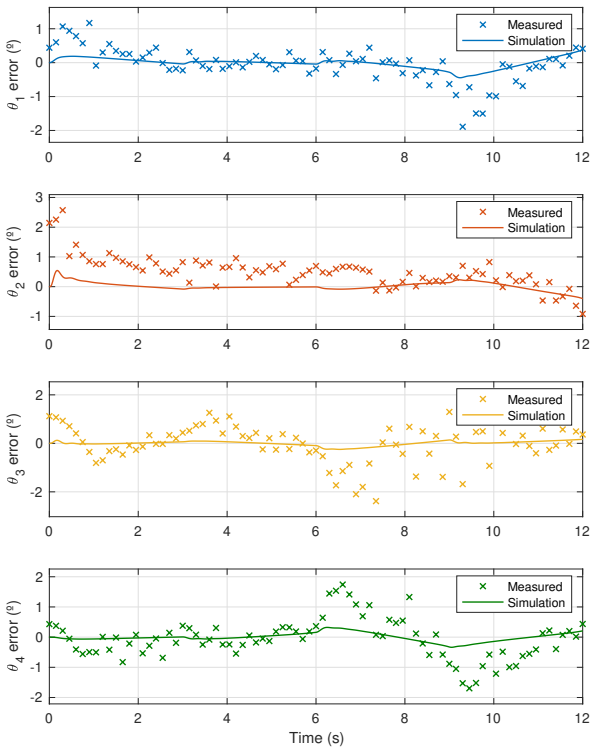

Figure 11. Joint angle tracking errors.

In order to better evaluate impedance control performance, the decoupled case has been adopted, where the 4×4 matrices $\mathbf{K}$, $\mathbf{B}$ and $\mathbf{M}$ are diagonal. In this case, the four output components of impedance model are equivalent to responses of decoupled second order linear differential equations. The transfer functions in (6) represent their behaviour in frequency domain.

$$\frac{\Delta x}{F_x} = \frac{\Delta y}{F_y} = \frac{\Delta z}{F_z} = \frac{\Delta \phi}{\tau_\phi} = K_n \frac{{\omega_n}^2}{s^2 + 2\xi\omega_n s + {\omega_n}^2}, \quad (6)$$

which ω_n is the natural frequency, ξ is the damping ratio and K_n is the static gain.

The impedance model in figure 4 was also discretized with a sampling frequency of 40 Hz and, as the developed force sensor does not measure torque, the ϕ dynamics has been neglected, and a fixed value has been assigned to ϕ in the impedance model.

6.2 Results

Preliminary results are presented in the video in `https://www.youtube.com/watch?v=vyzGGh-fPfE`.

In the following tests, the manipulator received a fixed virtual trajectory reference. During the test, a mass was hanged in the end effector for 10 s. The value of ϕ was set to 90°, so the force sensor measurement direction could be aligned to the gravitational acceleration. This setup ensured that all the contact force could be measured by the single axis force sensor available.

This test was performed for two different values of overshoot M_p. Figures 12 and 13 show the results for $M_p = 5\%$ and $M_p = 30\%$, respectively. In both cases, the settling time t_s and the constant gain K_n were keep at 5 s and 0.01, respectively. Notice that ω_n and ξ were calculated using M_p and t_s.

In both figures 12 and 13 the simulation and measurement for Δz were visibly close and presented the desired M_p and t_s characteristics. The differences between simulation and data for Δx and Δy are small and consistent with the position measurement resolution. In figure 12, one can observe sensor hysteresis, neglected during sensor calibration tests, since a residual F_z force has been measured even after the mass withdraw. Furthermore, figure 13 has shown noisier recorded forces than 12, as a consequence of bigger overshoot. This interference even caused the real data referent to Δz to divert considerably from simulation around 20 s.

7. CONCLUSION

The project confirmed that the implementation of impedance control based on position is a viable alternative for situations where a conventional position control loop is available, as in the case of servomotor actuators.

The utilization of second order transfer functions as impedance model proved to be very simple and efficient, although a suitable performance can be reached only with the prior knowledge of environment characteristics, for correct selection of impedance model parameters.

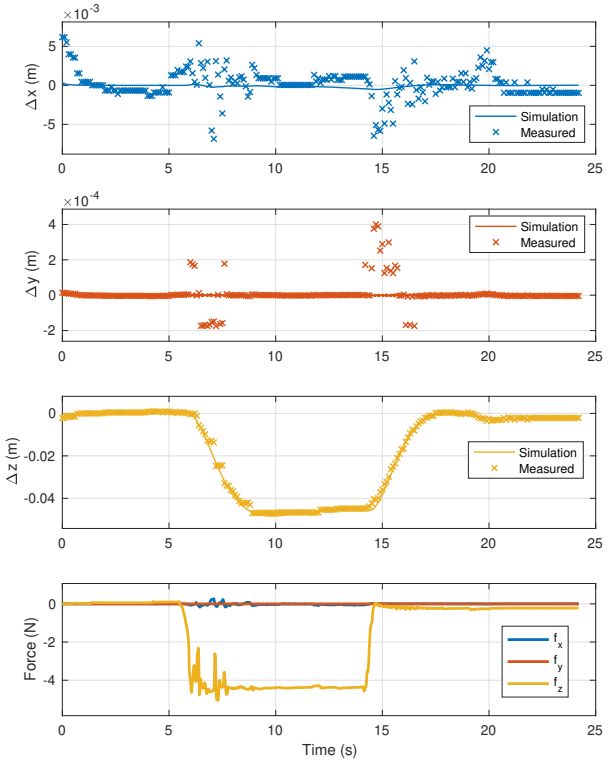

Figure 12. Cartesian displacements and forces - $M_p = 5\%$.

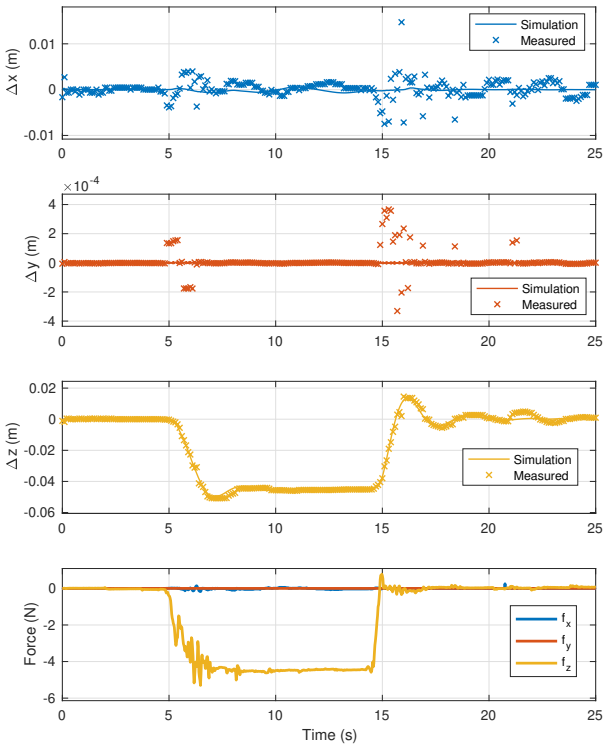

Figure 13. Cartesian displacements and forces - $M_p = 30\%$.

The main obstacles for improving position loop performance were the limited response time of actuators, as well as the quality of serial communication.

The force sensor is the most critical part of the entire control, as the impedance behaviour depends on the quality of force measurement for the chosen topology. Since commercial solutions did not fit in dimensional, deadline or budget constraints, the force sensor used in the final experiments has been developed with the available resources and presents a single measurement axis, what explains the simplifications adopted in the impedance loop.

Finally, future project extensions may include hardware and mechanical improvements and the study of adaptive tuning methods for impedance model parameters.

REFERENCES

Corke, P. (2017). *Robotics, Vision and Control*. Springer International Publishing.

Craig, J. (2013). *Introduction to Robotics: Mechanics and Control*. Pearson Education.

Faigl, J. and Čížek, P. (2019). Adaptive locomotion control of hexapod walking robot for traversing rough terrains with position feedback only. *Robotics and Autonomous Systems*, 116, 136–147.

Hogan, N. (1984). Impedance control: an approach to manipulation. In *1984 American Control Conference*, 304–313.

Ikeura, R. and Inooka, H. (1995). Variable impedance control of a robot for cooperation with a human. In *Proceedings of 1995 IEEE International Conference on Robotics and Automation*, volume 3, 3097–3102.

Jutinico, A.L., Jaimes, J.C., Escalante, F.M., Perez-Ibarra, J.C., Terra, M.H., and Siqueira, A.A.G. (2017). Impedance control for robotic rehabilitation: A robust markovian approach. *Frontiers in Neurorobotics*, 11.

Raibert, M. and Craig, J. (1981). Hybrid position/force control of manipulators. *Journal of Dynamic Systems, Measurement, and Control*, 103, 126–133.

Richardson, R., Brown, M., Bhakta, B., and Levesley, M. (2005). Impedance control for a pneumatic robot-based around pole-placement, joint space controllers. *Control Engineering Practice*, 13, 291–303.

ROBOTIS (2021). AX-12A. URL `http://emanual.robotis.com/docs/en/dxl/ax/ax-12a/`.

Shao, Z., Zheng, G., Efimov, D., and Perruquetti, W. (2015). Modelling and control of actuators with built-in position controller. *IFAC-PapersOnLine*, 48(11), 837–842.

Sharifi, M., Salarieh, H., Behzadipour, S., and Tavakoli, M. (2018). Beating-heart robotic surgery using bilateral impedance control: Theory and experiments. *Biomedical Signal Processing and Control*, 45, 256–266.

Song, P., Yu, Y., and Zhang, X. (2019). A tutorial survey and comparison of impedance control on robotic manipulation. *Robotica*, 37, 1–36.

Yarza, A., Santibanez, V., and Moreno-Valenzuela, J. (2011). Global asymptotic stability of the classical pid controller by considering saturation effects in industrial robots. *International Journal of Advanced Robotic Systems*, 8.